https://doi.org/10.5194/egusphere-2024-840
Preprint. Discussion started: 25 March 2024

Improving estimation of a record breaking East Asian dust storm emission with lagged aerosol Ångström Exponent observations

Yueming Cheng[1,2,3], Tie Dai[1,2*], Junji Cao[1], Daisuke Goto[4], Jianbing Jin[3], Teruyuki Nakajima[5], Guangyu Shi[1]

[1]State Key Laboratory of Numerical Modeling for Atmospheric Sciences and Geophysical Fluid Dynamics, Institute of Atmospheric Physics, Chinese Academy of Sciences, Beijing, China
[2]Collaborative Innovation Center on Forecast and Evaluation of Meteorological Disasters, Nanjing University of Information Science and Technology, Nanjing, China
[3]Collaborative Innovation Center of Atmospheric Environment and Equipment Technology, Jiangsu Key Laboratory of Atmospheric Environment Monitoring and Pollution Control (AEMPC), Nanjing University of Information Science and Technology, Nanjing, China
[4]National Institute for Environmental Studies, Tsukuba, Japan
[5]Tokyo University of Marine Science and Technology, Tokyo, Japan
Correspondence to: Tie Dai (daitie@mail.iap.ac.cn)

Abstract. A record-breaking East Asian dust storm over recent years occurred in March 2021. Ångström Exponent (AE) can resolve the particle size and is significantly sensitive to large aerosol such as dust. Due to lack of observation during dust storm and high uncertainty of satellite retrieved AE, it is crucial to estimate the dust storm emission using the lagged ground-based AE observations. In this study, the Aerosol Robotic Network (AERONET) observed hourly AEs are assimilated with the fixed-lag ensemble Kalman smoother and Weather Research and Forecasting model coupled with Chemistry (WRF-Chem) to optimize the simulated dust emission from 14 to 16 March 2021. The emission inversion results reveal that the dust emissions from the Gobi desert in the official WRF-Chem are significantly underestimated. Not only the temporal variation of simulated AE but also that of simulated aerosol optical thickness (AOT) can be improved through assimilating AE information. Compared to the assimilation with only AOT, the additional inclusion of AE doubles the dust emission and induces the extra 46.8% improvement of root mean square error (RMSE) between the simulated AOTs and the AERONET and independent Skynet Observation NETwork (SONET) observations. The optimized dust emission from Mongolia Gobi and China Gobi reach the peak value about 441.65 kt/hour and 346.87 kt/hour at 08:00 UTC on 14 March and at 19:00 UTC on 15 March, respectively. The additional inclusion of AE also best captures the magnitude and variations of aerosol vertical extinctions both in the westward and eastward pathways of dust transport.

1 Introduction

Mineral dust contributes the most abundant aerosol mass in the atmosphere. It affects the climate system by scattering and absorbing longwave and shortwave radiation as well as the contribution to the formation of cloud condensation nuclei (CCN) and ice-nucleating particles (INP) (Huang et al., 2006; IPCC AR6, Kok et al., 2018; Liu et al., 2020). Dust also carries

https://doi.org/10.5194/egusphere-2024-840
Preprint. Discussion started: 25 March 2024

organic matter and transports iron to ocean that is vital to ocean productivity and ocean-atmosphere CO_2 exchange, inducing the impacts on the cycles of dust and carbon (Shao et al., 2011). Dust deposition on snow surface can influence the snow albedo and modify the water cycle and energy budget (Wu et al., 2018; Kang et al., 2019; Wang et al., 2020). Moreover, severe dust storm can induce air pollution and affect human health (Chen et al., 2020).

East Asia, including the Taklimakan and Gobi deserts, is the world's second largest dust source, which occupies approximately 40% of the dust emissions in global (Satake et al., 2004; Kok et al., 2021) and accounts for 88% of the dust in China and neighbouring seas (Han et al., 2022). Although the dust activities in East Asia have declined recently (Wu et al., 2022), the unexpected extreme dust storm event occurred on 14 to 16 March 2021 reawakened widespread concern. Yin et al. (2022) explained that the loosened land and exiguous spring vegetation favours the lift of dust particles and the super-strong Mongolian cyclones provide great dynamic conditions for dust transport, which jointly cause the outbreak of super dust storms in this spring. However, quantitative research of this dust storm is limited, making it difficult to fully understand the whole dust cycle. Therefore, the accurate quantification of East Asian dust emission is critical.

Numerical simulation models are commonly used to study dust storm emission. However, due to insufficient knowledge of the actual dust mechanisms, more than ten fold diversity exists in simulated East Asian dust emissions among different models (Uno et al., 2006, Kok et al., 2021). Data assimilation, which feeds the observation information into numerical model, provides a top-down method for the optimization of the estimates of dust emissions. Yumimoto et al. (2008) assimilated the dust extinction coefficients derived from ground-based lidar network using four-dimensional variational (4D-Var) method, increasing the East Asian dust emissions by approximately 10 times. Sekiyama et al. (2010) developed an Ensemble Kalman Filter (EnKF) data assimilation system to jointly correct the global dust emissions and aerosol mixing ratios by assimilating the vertical observations from the Cloud-Aerosol Lidar and Infrared Pathfinder Satellite Observations (CALIPSO). Wang et al. (2012) constrained the amount and location of dust emissions in Taklimakan and Gobi deserts with the GEOS-Chem adjoint model by assimilating aerosol optical thicknesses (AOTs) from Moderate Resolution Imaging Spectroradiometer (MODIS). Based on the fixed-lag ensemble Kalman smoother technique, Schutgens et al. (2012) assimilated observations from AErosol RObotic NETwork (AERONET) and MODIS to estimate emissions for dust, sea salt, and carbonaceous aerosols. Yumimoto and Takemura (2015) performed inverse modeling of Asian dust with four-dimensional variational (4D-Var) data assimilation system and MODIS-retrieved AOT over ocean. Escribano et al. (2016) estimated dust emission and reduced their uncertainty over the Sahara desert and the Arabian Peninsula by assimilating MODIS AOT retrievals. Di Tomaso et al. (2017) used the four dimensional local ensemble transform Kalman filter (LETKF) to assimilate MODIS Dark Target and Deep Blue AOTs for improving dust analyses and forecasts in global. AOTs with high frequency from Himawari-8 geostationary satellite have been recently used for the inversion of dust storm emission with a reduced tangent linearization 4D-Var technique (Jin et al., 2019).

Except AOT, Ångström Exponent (AE) which measures the wavelength-dependence of AOT and is significantly sensitive to dust, is another key aerosol optical property. The AE at 440–870 nm is found lower than 0.2 for pure dust (Bi et al, 2016). Therefore, how will the assimilation of the AE observations affects the optimization of the dust emission? It becomes an

https://doi.org/10.5194/egusphere-2024-840
Preprint. Discussion started: 25 March 2024

open scientific question. Due to the large uncertainties of satellite retrieved AE, the high accuracy of the ground-based retrieved AE is crucial for data assimilation to optimize dust emissions. However, few studies have explored the potential benefits of assimilating ground-based AE on improving the estimate of dust emissions.

Motivated by this relatively unworked area, we develop a fixed-lag Ensemble Kalman smoother (EnKS) assimilation framework to constrain the extreme dust storm emission over East Asia from 14 to 16 March 2021. AOT and AE from AErosol RObotic NETwork (AERONET) are assimilated simultaneously, and the additional benefit of AE assimilation in estimating dust emission is also explored in this study.

In Section 2, we describe the assimilated and independent validation observations. Our dust emission inversion system and experimental design are presented in Section 3. Section 4 presents the emission inversion results and the validations by multi-sensor independent observations. The conclusions are given in Section 5.

2 Observation Data

2.1 Assimilated AERONET observations

AErosol RObotic NETwork (AERONET) is a federation of ground-based remote sensing aerosol network that collects aerosol optical observations with direct-sun photometers from various stations in global (https://aeronet.gsfc.nasa.gov) (Holben et al., 1998; Giles et al., 2019). Version 3 AOT data are divided into three levels according to the data quality procedures: Level-1 (unscreened), Level-1.5 (cloud-screened and quality-controlled), and Level-2 (quality-assured). In this study, the version 3 level 2 AOT at 550 nm and AE at 440-870 nm from AERONET are assimilated. AOT at 550 nm (τ) is obtained by logarithmic interpolation of the ones at 440 nm and 675 nm. AE is defined as the logarithms of AOT and wavelength, which is calculated based on AOTs at 440 and 870 nm. To ensure the accuracy, AE value is considered to be valid only when the AOTs at 440 nm and 870 nm both exceeds 0.05. The instantaneous observations are averaged every 1 hour, centering on the assimilation time slot. The observation error attributed to this averaged observation (ϵ) is calculated by a representation error (ϵ_r) and an observation error (ϵ_o) as $\epsilon^2 = \epsilon_r^2 + \epsilon_o^2$. The observation error in AOT is defined as 0.015 and the representation error of AOT is calculated as 0.055τ (Schmid et al., 1999). The representation error in AE is defined as 0.025 and the observation error of AE is estimated by propagating the observation error in AOT at 440 and 870 nm (Schutgens et al., 2010).

2.2 Independent SONET and CALIOP observations

Sun-Sky Radiometer Observation Network (SONET) is a ground-based aerosol network employing Cimel radiometer and multiwavelength polarization measurement to provide long-term columnar atmospheric aerosol properties over China (www.sonet.ac.cn) (Li et al., 2018). The aerosol optical related products including AOT, AE, fine-mode fraction (FMF) are graded into three levels: Level-1 (no triplet), Level-1.5 (cloudy), and Level-2 (no cloud). In this study, the level 2 AOT at

https://doi.org/10.5194/egusphere-2024-840
Preprint. Discussion started: 25 March 2024

550 nm and AE at 440-870 nm from SONET are used for independent validation and the instantaneous observations are also averaged every hour to generate hourly AOT and AE datasets.

Cloud-Aerosol Lidar with Orthogonal Polarization (CALIOP), aboard the CALIPSO satellite, is a dual-wavelength polarization lidar that performs observations of vertical structures of aerosols and clouds on the global scale (http://www-calipso.larc. nasa.gov) (Winker et al., 2007). In this study, the aerosol extinction coefficients at 532 nm in the CALIPSO lidar level 2 (L2) version 4.20 aerosol profile products over the altitude range below 12 km are also used for evaluation. The CALIPSO lidar level 2 version 4.20 Vertical Feature Mask (VFM) products, which include the feature types and subtype information, are used for aerosol discrimination (Omar et al., 2009; Cheng et al., 2019).

3 Model and data assimilation methodology

3.1 Forward model

Weather Research and Forecasting model coupled with Chemistry (WRF-Chem), which served as the forward model, is configured with the domain covering China with the 45 km horizontal resolution and 28 vertical levels. Due to the assimilated AERONET observations containing all the aerosol information, the Goddard Global Ozone Chemistry Aerosol Radiation and Transport (GOCART) aerosol scheme (chem_opt =300) is adopted to simulate the aerosols including both the dust and non-dust species (Chin et al., 2000, 2002). The Air Force Weather Agency (AFWA) dust emission scheme (dust_opt=3) is chosen for dust simulation. The mass mixing ratios of main aerosol components, including dust, sea salt, organic carbon, black carbon, and sulfate, are predicted. Other main selected physics are identical to those of Dai et al. (2019). To match the characteristics of East Asian dust, the fractions of the dust emission flux in the AFWA scheme are changed to 0.034, 0.187, 0.327, 0.163, and 0.309 for 0-2 μm, 2-3.6 μm, 3.6-6 μm, 6-12 μm, and 12-20 μm dust size bins (Su and Fung, 2015). Due to the original "aerosol chemistry to aerosol optical properties" module only redistributes dust mass from GOCART into MOSAIC 8 bins ranging from 0.039 μm to 10 μm, we increase the MOSAIC bins to 9 to include the dust aerosols in 10-20 μm size (Barnard et al., 2010; Ukhov et al., 2021). To compare with AERONET observed aerosol optical properties, the simulated ones are calculated assuming that the particles are spherical and internally mixed with all the simulated aerosol components (Barnard et al., 2010). The initial and lateral boundary meteorological conditions are from the NCEP Final (FNL) analysis. To reduce the uncertainties associated with the meteorological fields, the predicted wind (u, v), temperature (t), and specific humidity (q) by the WRF dynamical core are also nudged to the NCEP FNL analysis every 6 h for all layers (Dai et al., 2018).

3.2 Data assimilation framework

The adopted assimilation system, integrating measurements with model simulations, is based on the fixed-lag Ensemble Kalman Smoother (EnKS) with WRF-Chem (Dai et al., 2019). Twenty ensemble members are generated by only perturbing the dust emission, and the perturbation factor has a mean of 1 and a spread of 0.6 followed the lognormal distribution. The

https://doi.org/10.5194/egusphere-2024-840
Preprint. Discussion started: 25 March 2024

ensemble prediction dynamically estimates the covariance between the dust emission and the aerosol optical properties. The fixed-lag EnKS repeatedly corrects the dust emission at a specific time with the observations from that time step and subsequent times. In this study, the dust emission of WRF-Chem ensemble is optimized every 12 h with assimilation time window of 72 h. In other words, the dust emissions are optimized with the observations in current 12 h and subsequently lagged 60 h.

Four-dimensional local ensemble transform Kalman filter (4D-LETKF) is applied to solve the Kalman equations and find the maximum likelihood estimation of a state vector, which is here the posteriori dust emission $\bar{x}^a$ from the following formula:

$$\bar{x}^a = \bar{x}^b + X^b \bar{w}^a, \quad (1)$$

where $\bar{x}^b$ and X^b represent the ensemble mean of priori dust emission and the first guess ensemble perturbations, respectively. The weight matrix $\bar{w}^a$ is the Kalman gain, which determined the increment between the analysis and first guess as

$$\bar{w}^a = \tilde{P}^a (Y^b)^T R^{-1} (y^o - \bar{y}^b), \quad (2)$$

where R is the observation error covariance matrix; the y^o and $\bar{y}^b$ represent the assimilated hourly AOT and AE observations from AERONET and the first guess of the simulated AOT and AE observations averaged over the ensemble members; the WRF-Chem serves as the observation operator H to relate the priori dust emission to the first guess of the simulated observations, $\bar{y}^b = H(\bar{x}^b)$; the first guess ensemble perturbation matrix in observation space Y^b is calculated as $y^{b(i)} - \bar{y}^b, \{i = 1, 2, \dots, k\}$ with k ensemble members. The analysis error covariance is obtained as

$$\tilde{P}^a = \left[(k-1)I - Y^{b^T} R^{-1} Y^b\right]^{-1}, \quad (3)$$

where I is the identity matrix. The analysis ensemble perturbations X^a are obtained as

$$X^a = X^b W^a, \quad (4)$$

whose ith column is $x^a(i) - \bar{x}^a, \{i = 1,2, \dots, k\}$. In this study, the analysis ensemble by adding $\bar{x}^a$ to each of the columns of X^a forms the optimal dust emission for the ensemble forecast to produce the initial conditions for the next analysis. W^a is calculated as

$$W^a = [(k-1)\tilde{P}^a]^{1/2}. \quad (5)$$

4D-LETKF offers the advantage of selectively assimilating observations for a given grid point by employing localization in the horizontal, vertical, and temporal scales (Hunt et al., 2007; Gaspari and Cohn, 1999; Miyoshi et al., 2007). The horizontal localization factor is calculated as $f(r) = exp(-r^2/2\sigma^2)$, the factor is truncated at the 3.65 times of the localization length $\sigma = 600$ km in this study, and r is the distance between the observation and the center grid. The vertical and time localization is not applied in this study.

https://doi.org/10.5194/egusphere-2024-840
Preprint. Discussion started: 25 March 2024

3.3 Experimental design

To investigate the influences of AERONET AE assimilation on the dust emission inversion, two assimilation experiments are conducted from 00:00 UTC on 12 March 2021 to 00:00 UTC on 17 March 2021. The experiment named AOT DA only assimilates AERONET AOT observations, and the other experiment named AOT+AE DA assimilates both AOT and AE observations. The results from 00:00 UTC on 12 March 2021 to 23:59 UTC on 13 March 2021 are excluded in the analysis as the spin-up. The baseline experiment named FR does not assimilate any observations but otherwise share the same configuration with the assimilation experiments.

4 Results

4.1 Dust emission and simulated dust field

Fig. 1 shows the spatial distributions of the daily total dust emission, daily mean AOT, and daily mean AE for the three experiments in 14 March 2021, and these in 15 March and 16 March are given in Fig. 2 and Fig. 3. It is found that the dust emissions in the three experiments show generally consistent spatial and temporal patterns due to the dust emission perturbations are invariant with the model grid and time, however, the magnitudes of dust emission over Gobi desert on March 14 and 15 in DA experiments especially the AOT+AE DA are apparently larger than that in FR experiment. Due to the increments of dust emission with data assimilation, the simulated AOTs over the Gobi desert and its surrounding region with posterior dust emission in the two assimilation experiments are apparently higher than that in the FR experiment while the associated AEs are lower than that in the FR experiment. The highest AOT and AE in the FR experiment are concentrated in Southern China due to anthropogenic aerosols, while the highest AOT and lowest AE in the assimilation experiments are located in the Gobi desert due to dust. Although the major dust is emitted from the Gobi Desert in Mongolia, the high AOTs for the assimilation experiments are located in Inner Mongolia in China. The increased AOTs due to enlarged dust emissions in the assimilation experiments reveals that most part of the dust moves northeast on 14 March whereas most of the dust transports westward on 15 March. On 16 March, the eastward transported dust mainly moves to the southeast and affects the eastern China. The enlarged dust emissions in the assimilation experiments reduce the AE values especially over the dust source regions, and the spatial and temporal changes of AE between the FR and assimilation experiments are generally similar with that of AOT. Although northeast China on 15 March is dominated by dust, AE is generally higher than 0.8. It indicates that the primary particle in northeast China is mainly the fine mode dust which mixing with other anthropogenic aerosols during transporting. Due to the higher dust emissions induced by assimilating the additional AE observations, the AOT (AE) in the AOT+AE DA experiment is generally higher (lower) than that in the AOT DA experiment especially close to the source region.

https://doi.org/10.5194/egusphere-2024-840
Preprint. Discussion started: 25 March 2024

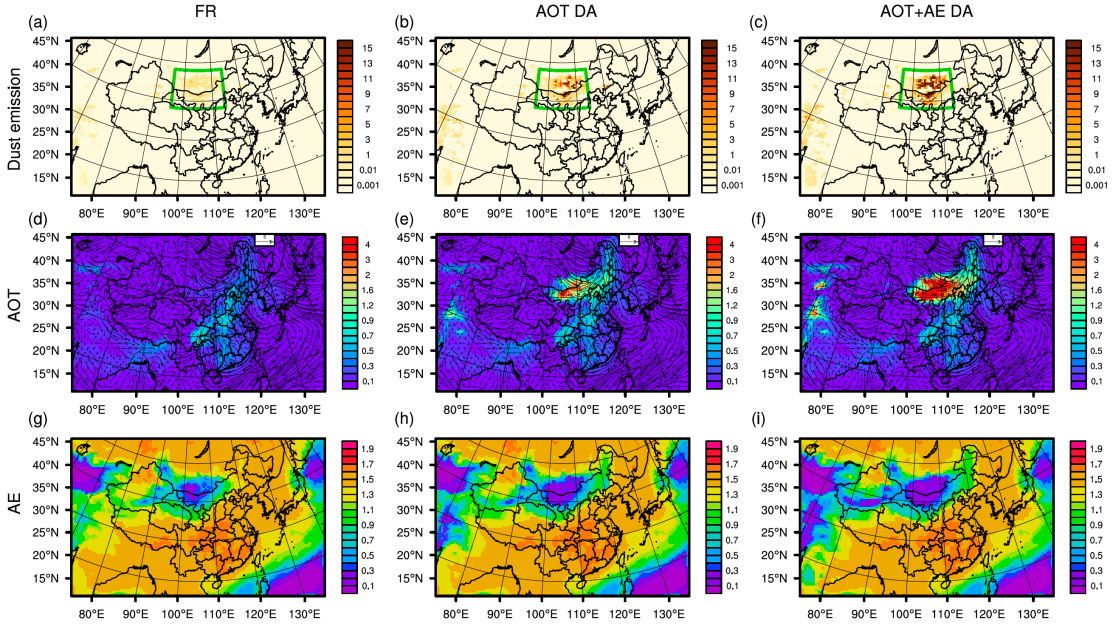

Figure 1. Spatial distributions of dust emission, aerosol optical thicknesses (AOTs), and Angstrom Exponent (AE) for FR, AOT DA, and AOT+AE DA experiments on 14 March 2021. The unit of dust emission is g/m^2/day. The green box represents the Gobi desert. Vectors in (a-c) represent the simulated surface wind field (m/s).

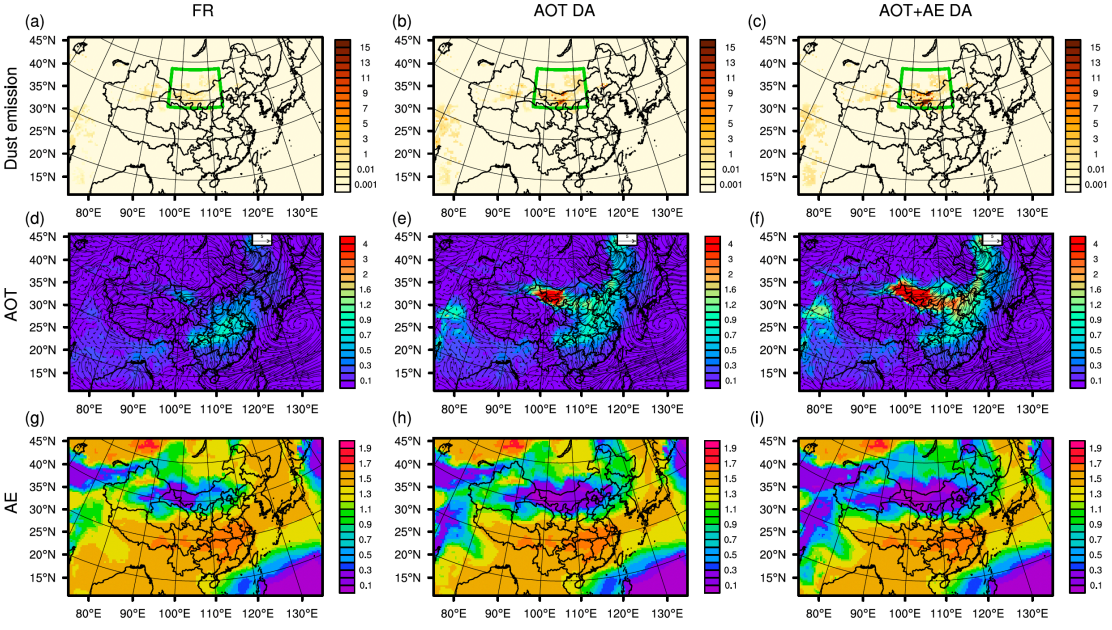

Figure 2. Same as Fig. 1 but on 15 March 2021.

https://doi.org/10.5194/egusphere-2024-840
Preprint. Discussion started: 25 March 2024

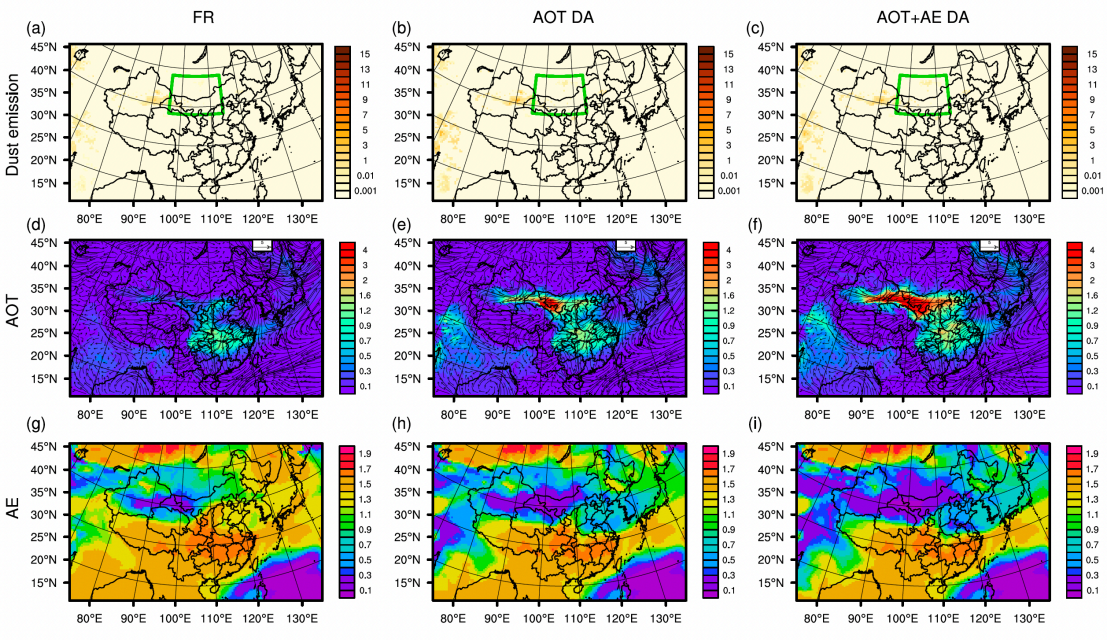

Figure 3. Same as Fig. 1 but on 16 March 2021.

The temporal variations of hourly accumulated dust emissions in Gobi desert of Mongolia and China simulated by FR, AOT DA, and AOT+AE DA experiments are further given in Fig. 4. The region of Gobi desert is marked as green box in Fig. 1. The dust in Gobi desert of Mongolia are mainly emitted from 06:00 UTC on 14 March to 18:00 UTC on 14 March while that in Gobi desert of China are from 12:00 UTC on 14 March to 12:00 UTC on 15 March. With respect to the Gobi desert in Mongolia, the hourly dust emission reaches the peak value of 19.71, 177.64, and 441.65 kt/hour at 08:00 UTC on 14 March for FR, AOT DA, and AOT+AE DA experiments. With respect to the Gobi desert in China, the hourly dust emission reaches the peak value of 10.25 kt/hour at 04:00 UTC on 15 March for FR experiment while the hourly dust emission reaches the peak value of 117.10 and 346.87 kt/hour at 19:00 UTC on 15 March for AOT DA and AOT+AE DA experiments. There are almost no dust emissions after 13:00 UTC on 15 March. In general, the dust emissions of the two assimilation experiments are significantly higher than that of FR experiment in the Gobi Desert. The increments of dust emission in Gobi desert are mainly occurred on 14-15 March, and it should be noted that there are no aerosol optical observations on those two days due to the large dust burden during the outbreak period of severe dust storm. It indicates that the increment of dust emission is induced by assimilating the observations after 2 days of dust storm outbreak. Both the dust emission flux in Gobi desert of Mongolia and China for the AOT+AE DA experiment are about three times as much as that in the AOT DA experiment. It reveals that the inclusion of AE observations has significant effect on the inversion of dust emission.

https://doi.org/10.5194/egusphere-2024-840
Preprint. Discussion started: 25 March 2024

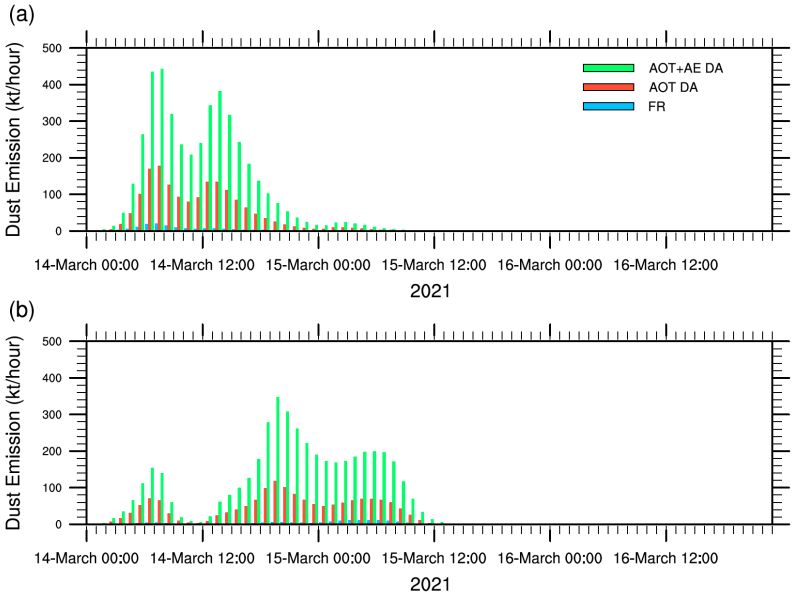

Figure 4. Time series of hourly accumulated dust emissions (units: kt/hour) for FR, AOT DA, and AOT+AE DA experiments during 14–16 March 2021 in Gobi desert (marked in Fig. 1) of Mongolia (a) and China (b).

3.2 Evaluation of simulated AOTs and AEs

To verify the inverted dust emission, the simulated hourly AOTs and AEs with the posterior and priori dust emissions are compared with the AERONET observations as the sanity check and compared with the SONET observed ones as the independent validations in Fig. 5. Due to the uncertainties of modelled covariance between dust emission and aerosol optical properties increase with the distance far away from the source region, only the observations within 2190 km (3.65 times of the localization length) of the East Asian dust source region are used for validation. Therefore, AERONET sites used here includes Beijing-CAMS (39.93°N, 116.32°E), Beijing (39.98°N, 116.38°E), Beijing_PKU (39.99°N, 116.31°E), and Beijing_RADI (40.00°N, 116.38°E), while SONET sites includes Beijing (40.00°N, 116.37°E), Jiaozuo (35.18°N, 113.20°E), Songshan (34.53°N, 113.09°E), and Zhengzhou (34.70°N, 113.66°E). To avoid the influences of non-dust aerosols, we only select the time when the AE observations are less than 0.6 for comparison (Bi et al., 2016). The total available collocated pair of AOTs and AEs is 47. It is found that the simulated AOTs are significantly underestimated while the simulated AEs are obviously overestimated for all the AERONET and SONET observations in the FR experiment. This demonstrates that the dust emission in FR experiment is obviously underestimated. The simulated AOT and AE with posterior dust emissions in both the two assimilation experiments are in better consistent with the observed ones. It is important to highlight that the improvement of simulated AOTs and AEs are benefited from utilizing the observations with a 2-day lag during dust emission inversion. In addition, the assimilated observations are in the downwind areas and more than 1000 km far from the dust source regions. Mean bias (BIAS), mean fractional error (MFE), and root mean square error (RMSE) of AOT (AE) are

https://doi.org/10.5194/egusphere-2024-840
Preprint. Discussion started: 25 March 2024

reduced by 34.1% (72.8%), 49.8% (37.4%), and 31.5% (68.1%) in the AOT DA experiment, while BIAS, MFE, and RMSE of AOT (AE) are further reduced by 63.6% (51.4%), 61.5% (31.6%), and 46.8% (30.1%) in the AOT+AE DA experiment. It is notable that not only the simulated AEs in the AOT+AE DA experiment are closest to the AE observations, but also the simulated AOTs are closest to the AOT observations. These further improvement of statistical metrics in the AOT+AE DA experiment proves that the inversion system with additional assimilation of AE can better optimize the dust source emissions and thus capture the aerosol spatiotemporal variation characteristics during dust transportation. The simulated AOTs and AEs align better with the observations at AERONET sites than those at SONET sites. It reveals that the simulated results with posterior dust emission perform better in the areas adjacent to the assimilated observations. Although the observations at SONET sites are not assimilated in the dust emission inversion, the simulated AOTs and AEs with posterior dust emission are more comparable to the SONET observations. It suggests that the background error covariances are well estimated in our data assimilation system, which is important for the dust emission inversion.

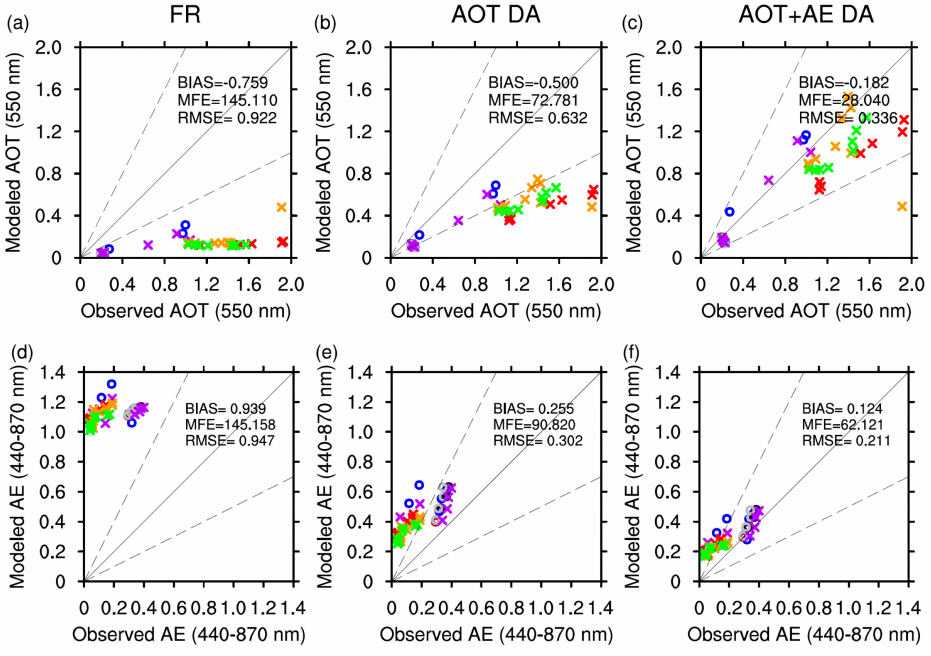

Figure 5. Scatter plots of AErosol RObotic NETwork (AERONET) and Skynet Observation NETwork (SONET) hourly AOTs versus the simulated ones at 550 nm for FR (a), AOT DA (b), and AOT+AE DA (c) experiments from 14 March to 16 March 2021. AERONET and SONET sites are illustrated by circle and cross. The blue, black, brown, and grey circle represent Beijing-CAMS, Beijing, Beijing_PKU, and Beijing_RADI AERONET sites, while the purple, red, orange, and green circle represent Beijing, Jiaozuo, Songshan, and Zhengzhou SONET sites. The solid black line is the 1:1 line and the dashed black lines correspond to the 1:2 and 2:1 lines. BIAS, MFE, and RMSE represent the mean bias, the mean fractional error, and the root mean square error, respectively. (d,e,f) Same as (a,b,c) but for AEs in the wavelength 440-870 nm.

https://doi.org/10.5194/egusphere-2024-840
Preprint. Discussion started: 25 March 2024

In Fig. 6, we selected two SONET sites to further evaluate the temporal evolutions of the simulated AOT and AE values for the three experiments with the independent SONET-retrieved ones. It is clear that the BIAS, RMSE, and CORR are all improved for the two assimilation experiments. Over the Beijing site, FR experiment produces the variations of aerosol size with a peak AE value at 06:00 UTC on 16 March, and both the two assimilation experiments correct the significant overestimations of AE, resulting in the improvements of the statistics. Over the Zhengzhou site, the simulated AOTs and AEs with prior dust emission are significantly underestimated and overestimated while the simulated AOTs and AEs in the AOT DA experiment are closer to the independent SONET observations from 00:00 UTC to 09:00 UTC on 16 March. Moreover, both the simulated AOTs and AEs in the AOT+AE DA experiment are more comparable to the independent observed ones with significantly reduced BIAS and RMSE. It indicates not only the simulated AEs but also the simulated AOTs can be improved through optimizing the dust emission estimates with including AE information. This further demonstrates that the AE observation is necessary for improving the dust emission inversion.

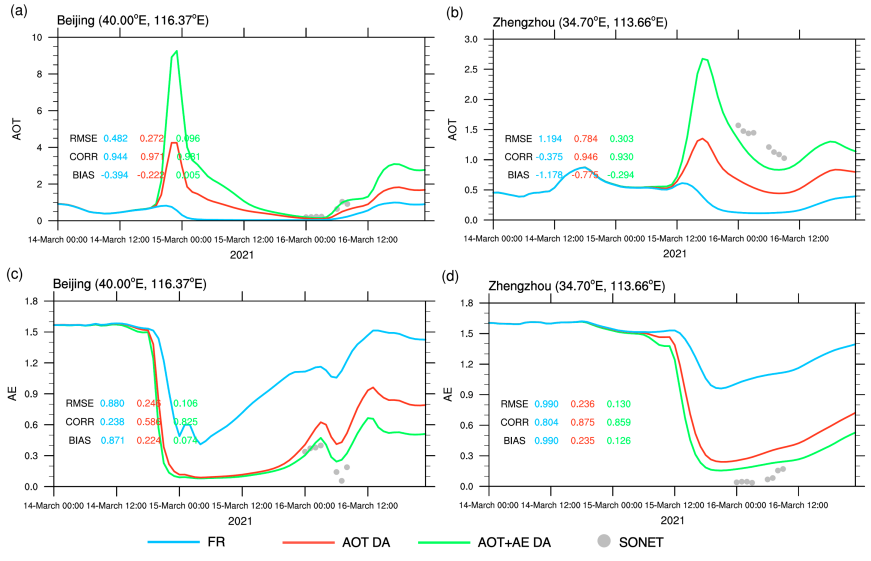

Figure 6. Hourly time series of the simulated AOTs for the three experiments and the observed ones over Beijing (a) and Zhengzhou (b) sites from 14 March to 16 March 2021. BIAS, RMSE, and CORR between the simulated AOTs and the SONET observed ones are also shown. (c,d) Same as (a,b) but for AEs in the wavelength 440-870 nm.

3.3 Evaluation of simulated aerosol vertical extinctions

To further evaluate the dust emission inversion, the simulated aerosol extinction coefficients for the three experiments are compared with the independent CALIOP observed ones in three CALIPSO orbit paths. Two paths near dust source region crosses the westward pathway of dust transport at 19:18:09 UTC on 15 March and the eastward pathway of dust transport at 05:55:25 (UTC) on 16 March, and one path is far away from the dust source region at 18:17:32 UTC on 16 March. As shown in Fig. 7, the vertical aerosols in path A are dominated by dust from 1 km to 12 km altitude. FR experiment can

https://doi.org/10.5194/egusphere-2024-840
Preprint. Discussion started: 25 March 2024

capture the observed aerosol vertical patterns, whereas it significantly underestimates the aerosol extinction coefficients near surface. Both the two assimilation experiments can reduce the underestimations, and the AOT+AE DA experiment performs better than the AOT DA experiment. Only AOT+AE DA experiment shows the more reasonable magnitude of aerosol extinction coefficients with values higher than 1 km^{-1} around surface from 35°N to 41°N and 0.1 km^{-1} from 2 km to 4 km around 40°N. It indicates that the assimilation of additional AE observations can better reproduce the features of aerosol vertical variations during dust transportation near the dust source region. In addition, it should be noted that the improvements of the aerosol extinctions with posterior dust emission on March 15 benefit from assimilating the time-lagged observations from downwind areas.

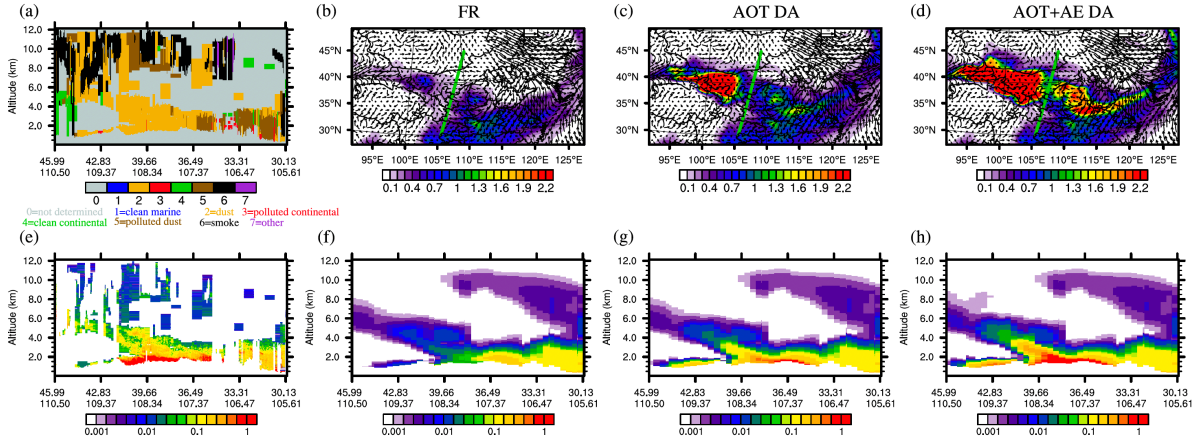

Figure 7. (a) Time-height cross section of CALIPSO-derived vertical aerosol subtypes in the CALIPSO orbit path at 19:18:09 (UTC) on 15 March 2021. The spatial distributions of the simulated AOTs at 550 nm at 19:00:00 (UTC) on 15 March 2021 in the FR (b), AOT DA (c), and AOT+AR DA (d) experiments. Vectors in (b-d) represent the simulated surface wind field (m/s). The green curve indicates the CALIPSO orbit path in (a). The CALIOP-observed aerosol extinction coefficients at 532 nm (km^{-1}) (e) and the simulated ones at 550 nm in the FR (f), AOT DA (g), and AOT+AR DA (h) experiments.

In Fig. 8, the dust transported from west to east is mainly concentrated in 4 km and FR generally reproduce this dust vertical structure with significant underestimations. Both the two assimilation experiments can improve the underestimations and the simulated aerosol extinctions are further consistent with the observed ones by the inclusion of AE information. CALIOP observed aerosol extinctions from 6 to 7 km around 41°N are higher than 1 km^{-1}, while the simulated aerosol extinctions for FR experiment are around 0.03 km^{-1}. AOT+AE DA experiment successfully reproduce the magnitude and variations of aerosol extinctions around 41°N.

https://doi.org/10.5194/egusphere-2024-840
Preprint. Discussion started: 25 March 2024

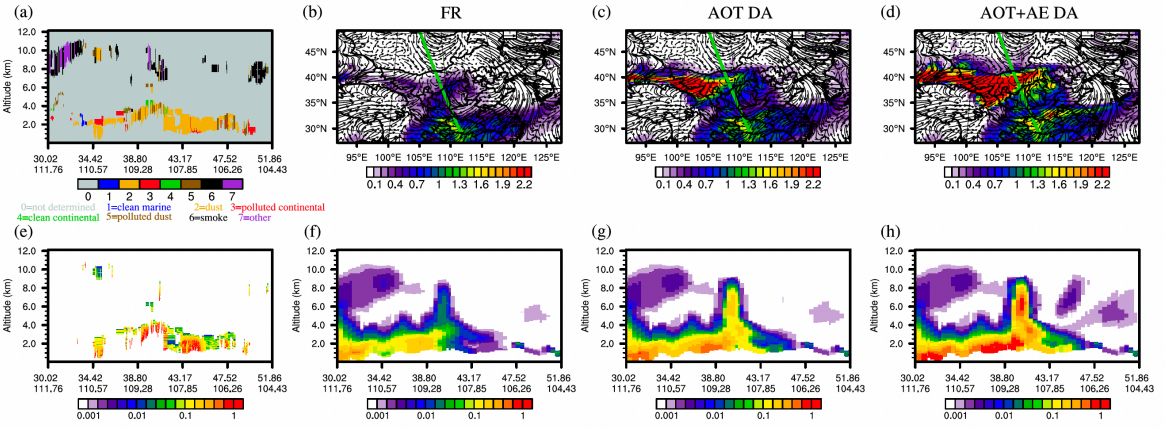

290 **Figure 8. Same as Fig. 7 but for the CALIPSO orbit path at 05:55:25 (UTC) on 16 March 2021. Vectors in (b-d) represent the simulated surface wind field (m/s).**

As shown in Fig. 9, the vertical aerosols in path B are also dominated by dust in all heights. Although FR experiment successfully reproduces the vertical structure of double dust-layers observed by CALIOP between 33°N to 43°N, the aerosol extinction coefficients are significantly underestimated around 4 km. Both the two assimilation experiments increase the
295 transported dust, diminishing the underestimation of aerosol extinction coefficients. It is also found that the aerosol extinction coefficients in AOT+AE DA experiment are more comparable to the CALIOP observations. This proves that the assimilation of additional AE observations can also better reproduce the features of dust vertical distributions in areas far away from the dust source region.

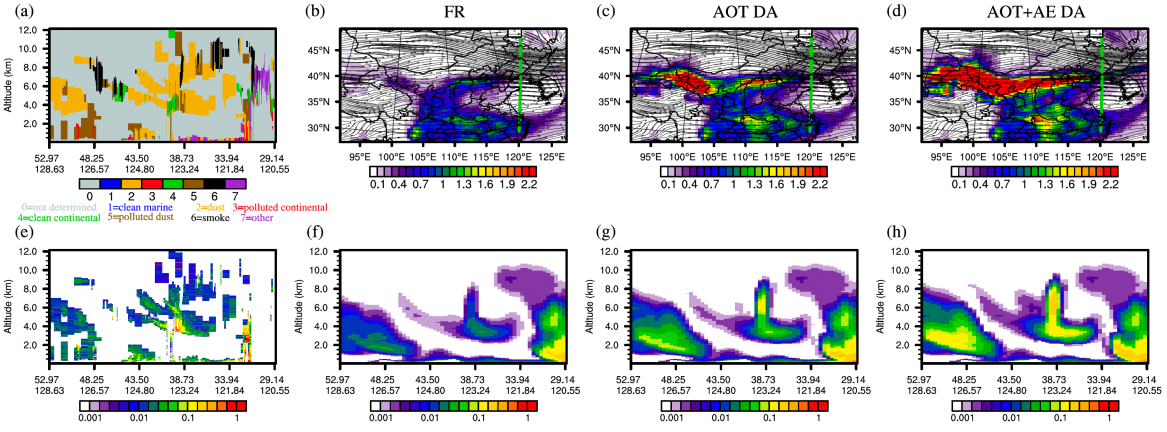

300 **Figure 9. Same as Fig. 7 but for the CALIPSO orbit path at 18:17:32 (UTC) on 16 March 2021. Vectors in (b-d) represent the simulated wind field (m/s) at 500 hpa.**

https://doi.org/10.5194/egusphere-2024-840
Preprint. Discussion started: 25 March 2024

4 Conclusions

To investigate the potential influences of the additional inclusion of Ångström Exponent (AE) assimilation on the dust emission inversion, the Aerosol Robotic Network (AERONET) ground-based aerosol optical thickness (AOT) and AE hourly observations after 2 days of a severe East Asian dust storm outbreak in March 2021 are assimilated in this study. The fixed-lag ensemble Kalman smoother with the Weather Research and Forecasting model coupled with Chemistry (WRF-Chem) is applied for the dust emission inversion. One assimilation experiment "AOT DA" is conducted through assimilating only AOT observations, while the other "AOT+AE DA" is conducted by assimilating both AOT and AE observations in tandem. The baseline experiment "FR" without assimilation is used for comparison.

The dust of this severe dust event is primarily emitted from the Gobi Desert in Mongolia, and primarily remains and affects the northern China. The priori dust emissions simulated with the WRF-Chem are significantly underestimated, therefore, the simulated AOTs (AEs) are apparently lower (higher) than the assimilated AERONET observed ones and the independent SONET ones. Although the CALIOP observed aerosol vertical structures including the double dust-layers between 33°N to 43°N are generally reproduced, the simulated aerosol extinctions with the priori dust emissions are significantly underestimated.

Emission inversion is successfully performed by the utilization of ground-based observations. Overall, the hourly dust emission in Mongolia reaches the peak value of 441.65 kt/hour at 08:00 UTC on 14 March and the dust emission in China reaches the peak value of 346.87 kt/hour at 19:00 UTC on 15 March for AOT+AE DA experiment. The simulated AOT and AE with posterior dust emission in both the two assimilation experiments are in better consistent with the observed ones. Compared to the assimilation of only AOT, the assimilation of additional AE doubles the dust emission and induces the extra 46.8% (30.1%) improvement of RMSE between the simulated AOTs (AEs) and the AERONET and independent SONET observations. It also best captures the magnitude and variations of aerosol vertical extinction coefficients both in the westward and eastward pathways of dust transport.

This study emphasizes the innovative superiority of additional AE assimilation in the dust emission inversion. To further explore the roles of the assimilated observations on the dust emission inversion and accurate simulation of dust life cycle, sensitivity experiments should be taken to quantify the influences of observation uncertainties and frequencies on the assimilation efficiency. The assimilation parameters such as spatial and temporal localization length are also important for dust emission inversion. In addition, the assimilated observations in this study include the aerosol optical properties from all the components, and assimilating only the dust information can be attempted in the future.

Code and data availability

All data used in this study is freely available from public data repositories. AERONET products are available from https://aeronet.gsfc.nasa.gov/new_web/download_all_v3_aod.html. SONET products are available from

https://doi.org/10.5194/egusphere-2024-840
Preprint. Discussion started: 25 March 2024

http://www.sonet.ac.cn/en/cpin/html/?194.html. CALIOP products are available from the NASA Langley Research Center–Atmospheric Sciences Data Center (ASDC).

Author contributions

YC conceived the study and designed the dust storm data assimilation. YC and TD performed the control and assimilation tests and carried out the data analysis. JC, DG, JJ, TN, and GS provided useful comments on the paper. YC prepared the manuscript with contributions from TD and all others co-authors.

Acknowledgments

This study was financially supported by the National Natural Science Funds of China (grant nos. 42175186, 42305088, 42375190), the China Postdoctoral Science Foundation (grant no. 2022M723091), the Special Research Assistant Project of the Chinese Academy of Sciences, the Open fund by Jiangsu Key Laboratory of Atmospheric Environment Monitoring and Pollution Control (KHK 2206), the Key Laboratory of Atmospheric Chemistry, China Meteorological Administration, LAC/CMA (grant no. 2022B05), the Youth Innovation Promotion Association CAS (grant no. 2020078), and the International Partnership Program of Chinese Academy of Sciences (grant no. 134111KYSB20200006). Model simulations were performed using NEC SX-Aurora TSUBASA supercomputers at NIES, Japan. We thank to the relevant researchers who provided AERONET, SONET, and CALIOP observations. We also thank the anonymous reviewers for their valuable comments and suggestions that improved the manuscript.

Competing interests

The contact author has declared that none of the authors has any competing interests.

References

Barnard, J.C.; Fast, J.D.; Paredes-Miranda, G.; Arnott, W.P.; Laskin, A. Technical note: Evaluation of the wrf-chem "aerosol chemical to aerosol optical properties" module using data from the milagro campaign. Atmos. Chem. Phys., 10, 7325–7340, 2010.

Bi, J., Huang, J., Holben, B., Zhang, G. Comparison of key absorption and optical properties between pure and transported anthropogenic dust over East and Central Asia. Atmospheric Chem. Phys. 16, 15501-15516. https://doi.org/10/gcc2r8, 2016

Chen, F., Chen, S., Zhang, X., Chen, J., Wang, X., Gowan, E. J., Qiang, M., Dong, G., Wang, Z., Li, Y., Xu, Q., Xu, Y., Smol, J. P., and Liu, J.: Asian dust-storm activity dominated by Chinese dynasty changes since 2000 BP, Nat Commun, 11, 992, https://doi.org/10.1038/s41467-020-14765-4, 2020.

Cheng, Y., Dai, T., Goto, D., Schutgens, N. A. J., Shi, G., and Nakajima, T.: Investigating the assimilation of CALIPSO global aerosol vertical observations using a four-dimensional ensemble Kalman filter, Atmos. Chem. Phys., 19, 13445–13467, https://doi.org/10.5194/acp-19-13445-2019, 2019.

https://doi.org/10.5194/egusphere-2024-840
Preprint. Discussion started: 25 March 2024

Dai, T., Cheng, Y., Zhang, P., Shi, G., Sekiguchi, M., Suzuki, K., et al. Impacts of meteorological nudging on the global dust cycle simulated by NICAM coupled with an aerosol model. Atmospheric Environment, 190, 99–115. https://doi.org/10.1016/j.atmosenv.2018.07.016, 2018.

Dai, Cheng, Goto, Schutgens, Kikuchi, Yoshida, et al. Inverting the East Asian Dust Emission Fluxes Using the Ensemble Kalman Smoother and Himawari-8 AODs: A Case Study with WRF-Chem v3.5.1. Atmosphere, 10(9), 543. https://doi.org/10.3390/atmos10090543, 2019.

Di Tomaso, E., Schutgens, N. A. J., Jorba, O., & Pérez García-Pando, C. Assimilation of MODIS Dark Target and Deep Blue observations in the dust aerosol component of NMMB-MONARCH version 1.0. Geoscientific Model Development, 10(3), 1107–1129. https://doi.org/10.5194/gmd-10-1107-2017, 2017.

Escribano, J., Boucher, O., Chevallier, F., & Huneeus, N. Subregional inversion of North African dust sources. Journal of Geophysical Research: Atmospheres, 121(14), 8549–8566. https://doi.org/10.1002/2016JD025020, 2016.

Gaspari, G., & Cohn, S. E. Construction of correlation functions in two and three dimensions. Quarterly Journal of the Royal Meteorological Society, 125(554), 723–757. https://doi.org/10.1002/qj.49712555417, 1999.

Giles, D. M., Sinyuk, A., Sorokin, M. G., Schafer, J. S., Smirnov, A., Slutsker, I., et al. Advancements in the Aerosol Robotic Network (AERONET) Version 3 database – automated near-real-time quality control algorithm with improved cloud screening for Sun photometer aerosol optical depth (AOD) measurements. Atmospheric Measurement Techniques, 12(1), 169–209. https://doi.org/10.5194/amt-12-169-2019, 2019.

Han, Y., Wang, T., Tang, J., Wang, C., Jian, B., Huang, Z., and Huang, J.: New insights into the Asian dust cycle derived from CALIPSO lidar measurements, Remote Sensing of Environment, 272, 112906, https://doi.org/10.1016/j.rse.2022.112906, 2022.

Holben, B. N., Eck, T. F., Slutsker, I., Tanré, D., Buis, J. P., Setzer, A., et al. AERONET—A Federated Instrument Network and Data Archive for Aerosol Characterization. Remote Sensing of Environment, 66(1), 1–16. https://doi.org/10.1016/S0034-4257(98)00031-5, 1998.

Huang, J., Lin, B., Minnis, P., Wang, T., Wang, X., Hu, Y., Yi, Y., and Ayers, J. K.: Satellite-based assessment of possible dust aerosols semi-direct effect on cloud water path over East Asia, Geophys. Res. Lett., 33, L19802, https://doi.org/10.1029/2006GL026561, 2006.

Hunt, B. R., Kostelich, E. J., & Szunyogh, I. Efficient data assimilation for spatiotemporal chaos: A local ensemble transform Kalman filter. Physica D: Nonlinear Phenomena, 230(1–2), 112–126. https://doi.org/10.1016/j.physd.2006.11.008, 2007.

IPCC. Climate Change 2021: The Physical Science Basis (eds Masson-Delmotte, V. et al.) (Cambridge Univ. Press, 2021).

Jin, J., Segers, A., Heemink, A., Yoshida, M., Han, W., & Lin, H. Dust Emission Inversion Using Himawari-8 AODs Over East Asia: An Extreme Dust Event in May 2017. Journal of Advances in Modeling Earth Systems, 11(2), 446–467. https://doi.org/10.1029/2018MS001491, 2019.

https://doi.org/10.5194/egusphere-2024-840
Preprint. Discussion started: 25 March 2024

Jin, J., Pang, M., Segers, A., Han, W., Fang, L., Li, B., et al. Inverse modeling of the 2021 spring super dust storms in East Asia. Atmospheric Chemistry and Physics, 22(10), 6393–6410. https://doi.org/10.5194/acp-22-6393-2022, 2022.

Kang, S., Zhang, Q., Qian, Y., Ji, Z., Li, C., Cong, Z., Zhang, Y., Guo, J., Du, W., Huang, J., You, Q., Panday, A. K., Rupakheti, M., Chen, D., Gustafsson, Ö., Thiemens, M. H., and Qin, D.: Linking atmospheric pollution to cryospheric change in the Third Pole region: current progress and future prospects, National Science Review, 6, 796–809, https://doi.org/10.1093/nsr/nwz031, 2019.

Kok, J. F., Ward, D. S., Mahowald, N. M., & Evan, A. T. Global and regional importance of the direct dust-climate feedback. Nature Communications, 9(1), 241. https://doi.org/10.1038/s41467-017-02620-y, 2018.

Kok, J. F., Adebiyi, A. A., Albani, S., Balkanski, Y., Checa-Garcia, R., Chin, M., et al. Contribution of the world's main dust source regions to the global cycle of desert dust (preprint). Atmospheric Chemistry and Physics. https://doi.org/10.5194/acp-2021-4, 2021.

Li, Z. Q., Xu, H., Li, K. T., Li, D. H., Xie, Y. S., Li, L., Zhang, Y., Gu, X. F., Zhao, W., Tian, Q. J., Deng, R. R., Su, X. L., Huang, B., Qiao, Y. L., Cui, W. Y., Hu, Y., Gong, C. L., Wang, Y. Q., Wang, X. F., Wang, J. P., Du, W. B., Pan, Z. Q., Li, Z. Z., and Bu, D.: Comprehensive Study of Optical, Physical, Chemical, and Radiative Properties of Total Columnar Atmospheric Aerosols over China: An Overview of Sun–Sky Radiometer Observation Network (SONET) Measurements, Bulletin of the American Meteorological Society, 99, 739–755, https://doi.org/10.1175/BAMS-D-17-0133.1, 2018.

Liu, Y., Zhu, Q., Hua, S., Alam, K., Dai, T., and Cheng, Y.: Tibetan Plateau driven impact of Taklimakan dust on northern rainfall, Atmospheric Environment, 234, 117583, https://doi.org/10.1016/j.atmosenv.2020.117583, 2020.

Miyoshi, T., Yamane, S., & Enomoto, T. Localizing the Error Covariance by Physical Distances within a Local Ensemble Transform Kalman Filter (LETKF). SOLA, 3, 89–92. https://doi.org/10.2151/sola.2007-023, 2007.

Omar, A. H., Winker, D. M., Kittaka, C., Vaughan, M. A., Liu, Z., Hu, Y., Trepte, C. R., Rogers, R. R., Ferrare, R. A., Lee, K.-P., Kuehn, R. E., and Hostetler, C. A.: The CALIPSO Automated Aerosol Classification and Lidar Ratio Selection Algorithm, JOURNAL OF ATMOSPHERIC AND OCEANIC TECHNOLOGY, 26, 21, 2009.

Satake, S., Uno, I., Takemura, T., Carmichael, G. R., Tang, Y., Streets, D., et al. Characteristics of Asian aerosol transport simulated with a regional-scale chemical transport model during the ACE-Asia observation. Journal of Geophysical Research: Atmospheres, 109(D19), 2003JD003997. https://doi.org/10.1029/2003JD003997, 2004.

Schutgens, N., Nakata, M., & Nakajima, T. Estimating Aerosol Emissions by Assimilating Remote Sensing Observations into a Global Transport Model. Remote Sensing, 4(11), 3528–3543. https://doi.org/10.3390/rs4113528, 2012.

Schmid, B., Michalsky, J., Halthore, R., Beauharnois, M., Harrison, L., Livingston, J., et al. Comparison of aerosol optical depth from four solar radiometers during the fall 1997 ARM intensive observation period. Geophysical Research Letters, 26(17), 2725–2728. https://doi.org/10.1029/1999GL900513, 1999.

Schutgens, N. A. J., Miyoshi, T., Takemura, T., & Nakajima, T. Applying an ensemble Kalman filter to the assimilation of AERONET observations in a global aerosol transport model. Atmos. Chem. Phys., 16, 2010.

https://doi.org/10.5194/egusphere-2024-840
Preprint. Discussion started: 25 March 2024

Shao, Y., Wyrwoll, K.-H., Chappell, A., Huang, J., Lin, Z., McTainsh, G. H., Mikami, M., Tanaka, T. Y., Wang, X., and Yoon, S.: Dust cycle: An emerging core theme in Earth system science, Aeolian Research, 2, 181–204, https://doi.org/10.1016/j.aeolia.2011.02.001, 2011.

Sekiyama, T. T., Tanaka, T. Y., Shimizu, A., & Miyoshi, T. Data assimilation of CALIPSO aerosol observations. Atmos. Chem. Phys., 11, 2010.

Wang, K. C., Dickinson, R. E., Wild, M., & Liang, S. Atmospheric impacts on climatic variability of surface incident solar radiation. Atmospheric Chemistry and Physics, 12(20), 9581–9592. https://doi.org/10.5194/acp-12-9581-2012, 2012.

Wang, T., Han, Y., Huang, J., Sun, M., Jian, B., Huang, Z., and Yan, H.: Climatology of Dust-Forced Radiative Heating Over the Tibetan Plateau and Its Surroundings, J. Geophys. Res. Atmos., 125, https://doi.org/10.1029/2020JD032942, 2020.

Su, L., & Fung, J. C. H. Sensitivities of WRF-Chem to dust emission schemes and land surface properties in simulating dust cycles during springtime over East Asia. Journal of Geophysical Research: Atmospheres, 120(21). https://doi.org/10.1002/2015JD023446, 2015.

Ukhov, A., Ahmadov, R., Grell, G., & Stenchikov, G. Improving dust simulations in WRF-Chem v4.1.3 coupled with the GOCART aerosol module. Geosci. Model Dev., 2021.

Uno, I., Wang, Z., Chiba, M., Chun, Y. S., Gong, S. L., Hara, Y., & Jung, E. (n.d.). Dust model intercomparison (DMIP) study over Asia: Overview.

Winker, D. M., Hunt, W. H., and McGill, M. J.: Initial performance assessment of CALIOP, Geophysical Research Letters, 34, https://doi.org/10.1029/2007GL030135, 2007.

Wu, C., Lin, Z., Shao, Y., Liu, X., and Li, Y.: Drivers of recent decline in dust activity over East Asia, Nat Commun, 13, 7105, https://doi.org/10.1038/s41467-022-34823-3, 2022.

Yin, Z., Wan, Y., Zhang, Y., and Wang, H.: Why super sandstorm 2021 in North China?, National Science Review, 9, nwab165, https://doi.org/10.1093/nsr/nwab165, 2022.

Yumimoto, K., Uno, I., Sugimoto, N., Shimizu, A., Liu, Z., & Winker, D. M. Adjoint inversion modeling of Asian dust emission using lidar observations. Atmospheric Chemistry and Physics, 8(11), 2869–2884. https://doi.org/10.5194/acp-8-2869-2008, 2008.

Yumimoto, Keiya, & Takemura, T. Long-term inverse modeling of Asian dust: Interannual variations of its emission, transport, deposition, and radiative forcing. Journal of Geophysical Research: Atmospheres, 120(4), 1582–1607. https://doi.org/10.1002/2014JD022390, 2015.